2D Materials Hot Paper

International Edition: DOI: 10.1002/anie.201814705
German Edition: DOI: 10.1002/ange.201814705

Active-Oxygen-Enhanced Homogeneous Nucleation of Lithium Metal on Ultrathin Layered Double Hydroxide

Zhenhua Li, Ke Liu, Kui Fan, Yusen Yang, Mingfei Shao, Min Wei, and Xue Duan*

Abstract: *The development of safe lithium-metal anodes is crucial for the next-generation rechargeable batteries. To stabilize Li metal anodes, pre-planting Li nucleation seeds on lithiophilic substrates is an efficient strategy to regulate initial nucleation process of Li metal. Now, activated ultrathin layered double hydroxide (U-LDHs) are reported as a promising lithiophilic 2D material to realize the uniform deposition of Li metal. The experimental studies and DFT calculations reveal that the active oxygen on U-LDHs provides abundant atomic-scale active sites for Li homogeneous nucleation and plating. Moreover, the lithiophilic properties of active oxygen is also related to its coordination environments. This work opens up an opportunity to more accurate regulation and understanding of Li nucleation from atomic-scale based on 2D ultrathin materials.*

Lithium-based batteries, especially Li-ion batteries (LIBs), have been widely used in various aspects of our daily life, such as electric vehicles, smart phones, and laptops.[1] However, the energy density of conventional LIBs are nearly approaching their theoretical value based on current commercially used cathode/anode materials (such as the graphite anode),[2] which cannot satisfy the increasing demands for high power application of the emerging cutting-edge electronic devices. In contrast, Li-metal batteries (LMBs) are considered as one of the most promising post-lithium-ion batteries because of the holy grail role of Li-metal anode with ultralow redox potential (−3.04 V vs. the standard hydrogen electrode) and very high theoretical specific capacity (3860 $mAh\,g^{-1}$).[3] Although rechargeable LMBs were initially proposed in the 1970s,[3d] their further applications in commercial batteries are hindered by the safety issue of Li-metal anode. The easy formation of Li dendrites owing to the uneven plating/stripping of Li metal not only induces the capacity loss and low Coulombic efficiency (CE) but also easily causes internal short circuiting.[4]

To stabilize the Li metal anode, considerable progress has been achieved from controlling the Li-deposition by introducting lithiophilic matrix[5] to regulate the side reactions by optimization of Li-metal/electrolyte interface.[6] Among them, preplanting Li nucleation seeds on lithiophilic substrates is becoming an efficient strategy to regulate initial nucleation process of Li metal and inhibit the formation of Li dendrites. Up to now, many materials, such as noble metals (for example, Au and Ag nanoparticles),[7] metal oxides (MgO, ZnO, Al_2O_3),[8] and nitrogen- and oxygen-doped carbons[9] have been successively identified with lithiophilic properties. These studies indicate a trend that uniformly dispersion of lithiophilic seeds on Li plating substrate at atomic scale is highly necessary for the homogeneous nucleation of Li. However, the current bulk structure, especially matal oxides, easy cause the formation of insulating layer, which is not conducive to efficient deposition of Li. Thus, the exploration for new lithiophilic nanomaterial with an easy regulated lithiophilic property and highly exposed active site is urgent to achieving high-performance LMBs.

Herein, we first develop an active-oxygen-rich surface based on ultrathin layered double hydroxide (denoted as U-LDH-O) to regulate the deposition/dissolution of Li metal for stable and efficient LMBs (Scheme 1). The interfacial engineering of U-LDH by a facile electrochemical strategy induces the efficient generation of active oxygen, which facilitates the homogeneous nucleation and dense growth of Li with effective dendrite suppression. Further experiments and density functional theory (DFT) calculations demonstrate that the atomically exposed active oxygen on the surface of LDH is thermodynamically favorable for the adsorption of Li atom and thus acts as real active site for the uniform nucleation and deposition of lithium metal. Furthermore, the ultrathin structure also promotes the adequate exposure of Li nucleation active sites and guarantees quick electron transfer between LDH-O and conductive substrate.

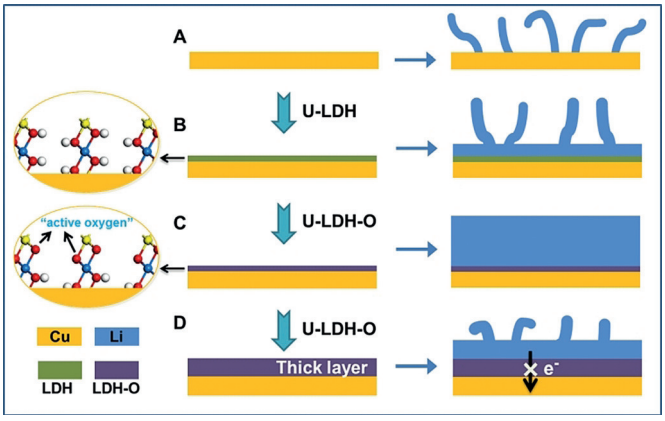

Scheme 1. Illustration of Li-metal growth on A) Cu substrates, B) U-LDH modified Cu substrates, C) thin U-LDH-O film modified Cu substrates, and D) thick U-LDH-O film modified Cu substrates.

[*] Z. Li, K. Liu, K. Fan, Y. Yang, M. Shao, M. Wei, X. Duan
State Key Laboratory of Chemical Resource Engineering
Beijing University of Chemical Technology
Beijing 100029 (China)
E-mail: shaomf@mail.buct.edu.cn

Supporting information and the ORCID identification number(s) for the author(s) of this article can be found under: https://doi.org/10.1002/anie.201814705.

The ultrathin CoFe-LDH nanosheets (U-LDH) with average diameter of 200–300 nm and continuous long-range homogeneity are vertically grown on Cu mesh via a facile electrosynthesis method (Supporting Information, Figure S1).[10] Active oxygen was then generated on the surface of U-LDH though an electrochemical oxidization process in 1M KOH solution (for details see the Experimental in the Supporting Information). The scanning electron microscope (SEM) image in Figure 1A shows that the ordered perpendicular array of U-LDH-O is well maintained, while the visible color has changed from yellow to dark (Supporting Information, Figure S1). Atomic force microscopy (AFM) images confirm the thickness of single U-LDH-O nanosheet is about 8 nm (Figure 1B). The cross-sectional SEM image shows that the thickness of whole U-LDH-O film on Cu substrate is about 300 nm (Figure 1C$_1$). EDS mapping analysis shows that Co, Fe, and O elements are uniformly distributed in the outer ring of Cu wire with a Co/Fe molar ratio of 1:1 (Figure 1C$_2$; Supporting Information, Figure S2). Raman spectra show that the original peak at 522 cm^{-1} (corresponding to the Co-OH phase) in the initial U-LDH is disappeared and replaced with two new peaks at 473 cm^{-1} and 546 cm^{-1} after electrochemical activation (Figure 1D), demonstrating the formation of a Co-OOH structure.[11] A nano-Fourier transform infrared (nano-FTIR) spectrum that was collected by micro-area AFM (Figure 1E; Supporting Information, Figure S3) shows that the peak at 1250 cm^{-2} for the interlayer carbonate is disappeared after electrochemical oxidization and the broad band between 3600 and 3200 cm^{-2} is also decreased significantly, demonstrating the removal of interlayer anion and reduction of hydroxyl group in LDH layers. The X-ray diffraction (XRD) illustrates that the removal of CO_3^{2-} causes the shrink of interlayer spacing of LDH because the (003) diffraction peak shift from 11.6° to 12.5° (Figure 1F). Thus, a electrochemical surface reconstruction is occurred during the electrochemical oxidation of U-LDH, in which the positively charged $[Co^{2+}Fe^{3+}(OH)_4]^+$ hydroxide monolayers of U-LDH is converted to electroneutral $[Co^{3+}Fe^{3+}(OOH)_2]^0$ oxyhydroxide monolayers through the deprotonating process. This reconstruction causes the successful formation of highly dispersed terminal-O on the surface of U-LDH-O nanosheets (as shown in Scheme 1C). FTIR spectra with deuterated chloroform ($CDCl_3$) as a probe molecule directly reveal the existence of highly active terminal-O (Supporting Information, Figure S4), which is denoted as active oxygen.

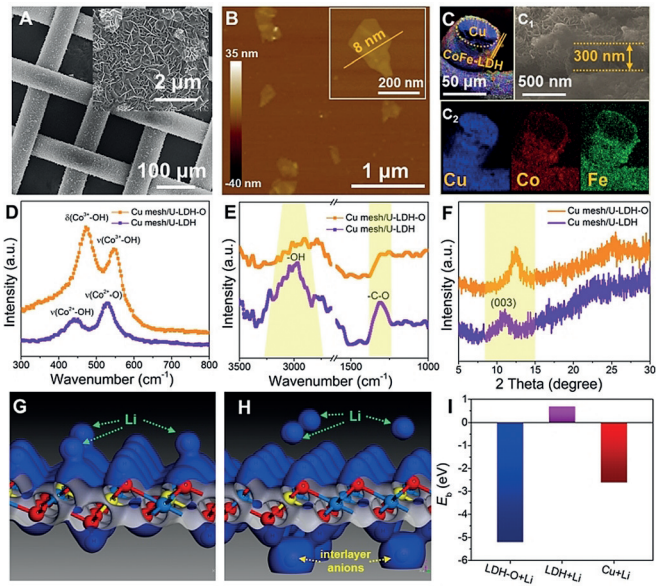

Figure 1. A) SEM images of Cu mesh/U-LDH-O with different magnification. B) AFM topograph of U-LDH-O nanosheets. C) SEM image and EDS mapping of Cu mesh/U-LDH-O: C$_1$ is the cross-sectional SEM image and C$_2$ is the corresponding EDS mapping result of Cu, Co, Fe, and their overlay images. D) Raman spectra, E) nano-FTIR spectra, and F) XRD pattern of U-LDH and U-LDH-O on Cu mesh. G),H) Electron density of Li atom adsorption on (G) LDH-O and (H) LDH. I) The calculated adsorption energies of U-LDH-O + Li, U-LDH + Li, and Cu + Li.

In our previous work, we found that the oxygen (C=O) on carbon nanotube surface can act as efficient lithiophilic site to guide Li-metal nucleation and growth.[12] Inspired by this, the active oxygen in U-LDH-O may also be active site for Li-metal deposition. To prove this hypothesis, DFT calculation is initially utilized to study the Li adsorption behavior of U-LDH-O. Figure 1G,H and the Supporting Information, Figure S5 are the electron 3D charge density plot for Li atom over LDH-O, LDH and metallic Cu substrate. It can be seen apparently that the Li atom is facilely absorbed over the terminal-O site of LDH-O with strongly electronic overlap (Figure 1G), while it is mutually exclusive between Li atom and LDH (Figure 1H). This demonstrates that the surface active oxygen of LDH-O is thermodynamically favorable for Li atom adsorption. Moreover, the calculated adsorption energies show that Li atom adsorbed LDH-O exhibits the most negative adsorption energies (LDH-O + Li; −5.20 eV) than that of Li atom over LDH (LDH + Li; 0.68 eV) and Cu substrate (Cu + Li; −2.61 eV) (Figure 1I). The above results indicate that the U-LDH-O is a promising lithiophilic material for homogenous deposition of Li-metal.

To demonstrate the efficiency of U-LDH-O modified Cu substrate for Li nucleating and plating, we investigate the Li-metal deposition behaviors on U-LDH-O, U-LDH, as well as pure Cu mesh substrate using a galvanostatic electrodeposition method in 2032-type coin cells. Figure 2A is the voltage–capacity curve of these three electrodes for Li deposition at a current density of 0.5 mA cm^{-2}. The nucleation and plateau overpotential are employed to evaluate the procedures of Li nucleation and growth. Obviously, the voltage curve of U-LDH-O electrode exhibits a smooth voltage dip at the nucleation stage with a small gap between nucleation and plateau overpotential (only 16.2 mV), which is obviously smaller than that of U-LDH (28.3 mV) as well as Cu mesh substrate (74.6 mV). This can be attributed to the high lithiophilic property of U-LDH-O that facilitates the Li nucleation.

The morphology change of the U-LDH-O electrode after Li-plating and stripping was also studied. As shown in Figure 2B and the Supporting Information, Figure S6A, dense and small Li nucleus appears on the surface of U-

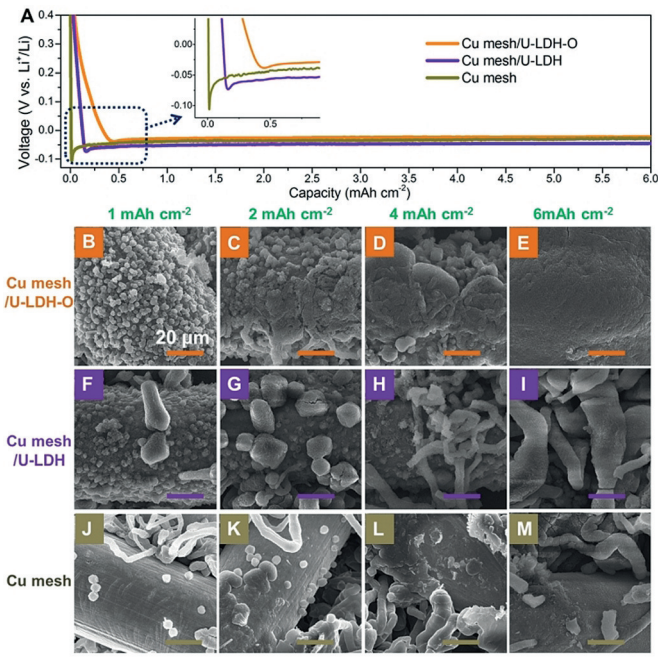

Figure 2. A) The voltage–time curves during Li nucleation on Cu mesh/U-LDH-O, Cu mesh/U-LDH, and Cu mesh. SEM image of Li-metal plating on these three substrates with different plating capacity: B)–E) Cu mesh/U-LDH-O, F)–I) Cu mesh/U-LDH, J)–M) pure Cu mesh. Scale bar: 20 μm.

LDH-O at a low Li plating capacity (1 mAh cm^{-2}). Then, the Li nucleus is intergradation (2 mAh cm^{-2}; Figure 2C; Supporting Information, Figure S6B) and the whole skeleton of U-LDH-O/Cu mesh electrode is uniformly covered with dense Li (4 mAh cm^{-2}; Figure 2D; Supporting Information, Figure S6C). Finally, Li gradually fills up the hollows of substrate and forms a smooth surface on the electrode (6 mAh cm^{-2} and 8 mAh cm^{-2}; Figure 2E; Supporting Information, Figure S6D,E). Moreover, the U-LDH-O electrode can be recovered after the Li stripping (Supporting Information, Figure S6F). In contrast, Li is non-uniformly nucleated and forms some large Li nanoparticles (> 20 μm) on the U-LDH sample (1 mAh cm^{-2}; Figure 2F; Supporting Information, Figure S7A). The Li nanoparticles grow bigger (2 mAh cm^{-2}; Figure 2G; Supporting Information, Figure S7B) and stocky Li dendrites are generating on the Li nanoparticles at 4 mAh cm^{-2} (Figure 2H; Supporting Information, Figure S7C). Finally, the whole surface of U-LDH electrode is covered with thick Li dendrites (6 mAh cm^{-2}; Figure 2I; Supporting Information, Figure S7D). Li is also hard to nucleate on a pure Cu mesh substrate, causing the formation of long and thin Li dendrites (Figure 2J–M; Supporting Information, Figure S8). The same phenomenon is also observed on the Cu foil substrate (Supporting Information, Figure S9). Besides, the moderate thickness of U-LDH-O is necessary to achieve uniform deposition of Li, and the thick U-LDH-O modified Cu mesh is unfavorable for Li plating owing to the blocked electronic transmission (Supporting Information, Figure S10).

To evaluate the reversibility of Li-metal during continuous stripping/plating operation, we examined the coulombic efficiency (CE) of U-LDH-O electrode, which is calculated from the voltage–capacity curves. As shown in Figure 3A and the Supporting Information, Figure S11, the U-LDH-O exhibits fairly high and stable CE of 98.5% at current density

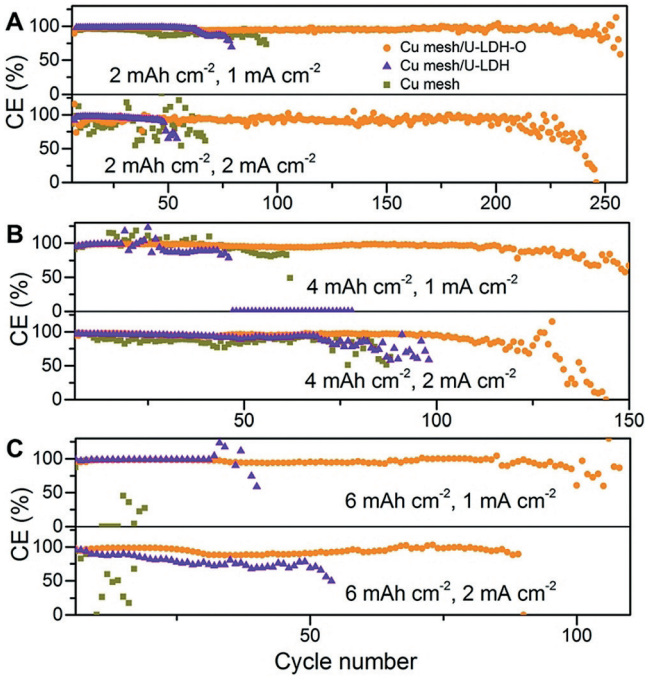

Figure 3. Coulombic efficiency of U-LDH-O, U-LDH, and Cu mesh substrate with different current density and Li plating capacity: A) 2 mAh cm^{-2}, B) 4 mAh cm^{-2}, C) 6 mAh cm^{-2}.

of 1 mA cm^{-2} and 97.3% at a current density of 2 mA cm^{-2} after 200 cycles at an areal capacity of 2 mAh cm^{-2}. In contrast, the U-LDH shows rapid CE decay to 69.6% after just 70 cycles at 1 mA cm^{-2} and to 65.0% within 45 cycles at 2 mA cm^{-2}. The CE of Cu mesh substrate also decays rapidly to 70.2% at 1 mA cm^{-2} and 61.5% under 2 mA cm^{-2} after 90 cycles. When the cycling capacity increased to 4 mAh cm^{-2} (Figure 3B), the CE of U-LDH-O still reach stable at 97.6% at 1 mA cm^{-2} and 96.3% at 2 mA cm^{-2} after 100 cycles. However, the CE of U-LDH and Cu mesh is oscillated rapidly and dropped to below 70% just within 70 cycles. Impressively, when the cycling capacity is as high as to 6 mAh cm^{-2} (Figure 3C), the U-LDH-O electrode retains a stable CE (> 95%) after 80 cycles at both 1 mA cm^{-2} and 2 mA cm^{-2}, whereas more apparent CE decay with the U-LDH and Cu mesh has been observed. The CE of the U-LDH dramatically decreases to 58.1% after 40 cycles at 1.0 mA cm^{-2} and to 49.7% after 20 cycles at 2.0 mA cm^{-2}, respectively. Furthermore, the CE of bare Cu mesh shows prominent and irregular fluctuations during the Li deposition and stripping cycles owing to partial short circuits originating from the appearance of Li dendrites. Moreover, the U-LDH-O@Li symmetrical cell delivers a lower deposition potential of 23 mV in the initial cycle and can be stabled over 200 cycles (29 mV in the 200th cycle), whereas the symmetrical cell of the bare Li exhibits a much higher Li stripping/plating overpotential of > 50 mV and short circuit occurred at the 160th cycle

(Supporting Information, Figure S12). These results indicate the outstanding reversibility and high Li utilization of the U-LDH-O electrode.

To better understanding the Li nucleation mechanism, we further investigated the relationship between the coordination environment of active oxygen and Li deposition. In LDH-O, the terminal-O is bonded with inner Co and/or Fe to form oxygen-bridged metal motifs. Thus, the coordination structure of active oxygen can be adjusted by changing the Co/Fe molar ratio on the oxyhydroxide monolayers. As shown in Figure 4 A–C, there are three possible active oxygen on the (001) surface of the LDH-O model: I) an O atom bound to three Co atom (Co/Fe > 2; Figure 4 A); II) an O atom bound to two Co atom and one Fe atom (Co/Fe = 2; Figure 4 B); and III) an O atom bound to one Co atom and two Fe atom (Co/Fe = 1; Figure 4 C). It is found that the O atom bound three Fe atom in LDH-O is not possible due to the occurrence of structure change during the deprotonating process of LDH (Co/Fe < 1; Supporting Information, Figure S13). Based on the above information, we calculate the adsorption energy between Li atom and these three type active oxygen. The results show that the terminal-O (III) possesses the most negative adsorption energies of −5.20 eV than that of terminal-O (I) (−5.01 eV) and terminal-O (II) (−5.08 eV), indicating that the O atom bound one Co atom and two Fe atoms in U-LDH-O is the best Li adsorption site. This can be illustrated by the valence electron structures of metal ions in Co-O-Fe and Co-O-Co. As shown in Figure 4 D and 4E, Fe^{3+} ions have fewer electrons in π-symmetry (t_{2g}) d-orbitals than $Co^{3+/2+}$ ions, which results that Fe^{3+} in Co-O-Fe increases the electron-donating ability of the t_{2g} lone pairs of bridging oxygen atoms,[13] and thus causes the formation of electron-deficient oxygen. This thereby inducts the electron transfer from Li to terminal-O, forming stronger Li-O adsorption and enhances the lithiophilic properties.

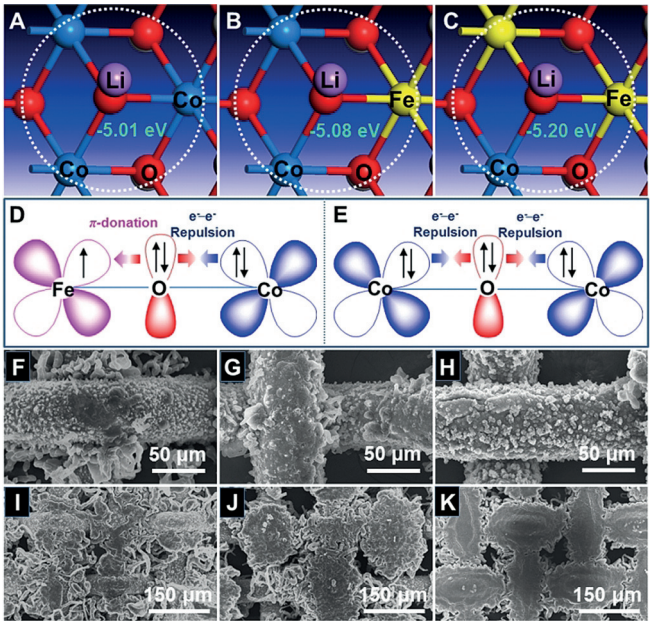

Figure 4. Atomic model of Li atom adsorption on LDH-O with different oxygen-bridged metal motifs: A) O atom bond three Co atom, B) O atom bound two Co atom and one Fe atom, C) O atom bond one Co atom and two Fe atom. D),E) Illustrations of the electronic coupling structures for D) Co-O-Fe and E) Co-O-Co. SEM images of Li plating on F),I) Cu mesh/Co_4Fe_1-LDH-O, G),J) Cu mesh/Co_2Fe_1-LDH-O, and H),K) Cu mesh/Co_1Fe_1-LDH-O with different Li plating capacity: F)–H) 1 mAh cm^{-2}, I)–K) 6 mAh cm^{-2}.

We further studied the Li plating behavior on CoFe-LDHs with different Co/Fe molar ratio (Supporting Information, Figure S14). The SEM images show that Li is more homogeneous nucleation on Co_1Fe_1-LDH-O and gradually forms a flat surface (Figure 4 H and K). However, Li cannot be so uniformly plated to form smooth surface on Co_2Fe_1-LDH-O (Figure 4 G and J). Furthermore, some Li dendrites are even generated for Co_4Fe_1-LDH-O (Figure 4 F and I). The Li dendrite growth is more serious on γ-CoOOH (Supporting Information, Figure S15 A–C) and γ-FeOOH electrodes (Supporting Information, Figure S15 D–F) owing to the absence of Co-O-Fe structure. Based on above results, we can recognize that the terminal-O with Co-O-Fe structure is more favorable for the adsorption and nucleation of Li.

In summary, active-oxygen-containing LDH has been successfully proven to be a good lithiophilic 2D nanomaterial to improve the Li deposition behavior, where Li-metal can be uniformly deposited on the U-LDH-O electrode to form flat surface with good reversibility. Both experimental studies and DFT calculations reveal that the terminal-O on LDH-O plays a key role for the homogeneous nucleation and plating of Li-metal, which acts as real active site. Moreover, the lithiophilic property of terminal-O is also related to its coordination environments, where the Co-O-Fe structure in LDH-O largely facilitates the Li nucleation. This work first reports the earth-abundant transition-metal (oxy)hydroxides as a promising surface modifier to guide the Li-metal uniform stripping/plating, which helps us better understand the Li growth mechanism and improves the stability of lithium metal anodes.

Acknowledgements

This work was supported by the National Natural Science Foundation of China (21601011, 21871021, and 21521005), the National Key Research and Development Programme (2017YFA0206804), and the Fundamental Research Funds for the Central Universities (XK1802-6).

Conflict of interest

The authors declare no conflict of interest.

Keywords: active oxygen · layered double hydroxides · Li metal · lithiophilic properties · ultrathin 2D materials

How to cite: *Angew. Chem. Int. Ed.* **2019**, *58*, 3962–3966
Angew. Chem. **2019**, *131*, 4002–4006

[1] a) S. Chu, A. Majumdar, *Nature* **2012**, *488*, 294; b) K. Amine, R. Kanno, Y. Tzeng, *MRS Bull.* **2014**, *39*, 395; c) B. Dunn, H. Kamath, J.-M. Tarascon, *Science* **2011**, *334*, 928.

[2] a) H. Ren, J. Sun, R. Yu, M. Yang, L. Gu, P. Liu, H. Zhao, D. Kisailus, D. Wang, *Chem. Sci.* **2016**, *7*, 793; b) H. Ren, R. Yu, J. Wang, Q. Jin, M. Yang, D. Mao, D. Kisailus, H. Zhao, D. Wang, *Nano Lett.* **2014**, *14*, 6679; c) Y. Yang, X. Liu, Z. Zhu, Y. Zhong, Y. Bando, D. Golberg, J. Yao, X. Wang, *Joule* **2018**, *2*, 1075.

[3] a) J. M. Tarascon, M. Armand, *Nature* **2001**, *414*, 359; b) W. Xu, J. Wang, F. Ding, X. Chen, E. Nasybulin, Y. Zhang, J. G. Zhang, *Energy Environ. Sci.* **2014**, *7*, 513; c) J. B. Goodenough, Y. Kim, *Chem. Mater.* **2010**, *22*, 587; d) X.-B. Cheng, R. Zhang, C.-Z. Zhao, Q. Zhang, *Chem. Rev.* **2017**, *117*, 10403; e) S. Wu, Z. Zhang, M. Lan, S. Yang, J. Cheng, J. Cai, J. Shen, Y. Zhu, K. Zhang, W. Zhang, *Adv. Mater.* **2018**, *30*, 1705830.

[4] a) H. Kim, G. Jeong, Y. U. Kim, J. H. Kim, C. M. Park, H. J. Sohn, *Chem. Soc. Rev.* **2013**, *42*, 9011; b) D. Lu, Y. Shao, T. Lozano, W. D. Bennett, G. L. Graff, B. Polzin, J. Zhang, M. H. Engelhard, N. T. Saenz, W. A. Henderson, P. Bhattacharya, J. Liu, J. Xiao, *Adv. Energy Mater.* **2015**, *5*, 1400993; c) C. Monroe, J. Newman, *J. Electrochem. Soc.* **2005**, *152*, A396; d) L. Grande, E. Paillard, J. Hassoun, J. B. Park, Y. J. Lee, Y. K. Sun, S. Passerini, B. Scrosati, *Adv. Mater.* **2015**, *27*, 784.

[5] a) J. E. Cloud, Y. Wang, X. Li, T. S. Yoder, Y. Yang, Y. Yang, *Inorg. Chem.* **2014**, *53*, 11289; b) H. Kim, C.-Y. Chou, J. G. Ekerdt, G. S. Hwang, *J. Phys. Chem. C* **2011**, *115*, 2514; c) Z. Liang, D. Lin, J. Zhao, Z. Lu, Y. Liu, C. Liu, Y. Lu, H. Wang, K. Yan, X. Tao, Y. Cui, *Proc. Natl. Acad. Sci. USA* **2016**, *113*, 2862.

[6] a) Y. Lu, Z. Tu, L. A. Archer, *Nat. Mater.* **2014**, *13*, 961; b) Y. Yan, Y. X. Yin, Y. G. Guo, L. J. Wan, *Sci. China. Chem.* **2014**, *57*, 1564; c) Z. Y. Tu, Y. Y. Lu, L. Archer, *Small* **2015**, *11*, 2631; d) M. Wu, Z. Wen, J. Jin, B. V. Chowdari, *ACS Appl. Mater. Interfaces* **2016**, *8*, 16386; e) J. Qian, W. A. Henderson, W. Xu, P. Bhattacharya, M. Engelhard, O. Borodin, J. G. Zhang, *Nat. Commun.* **2015**, *6*, 6362.

[7] a) K. Yan, Z. Lu, H.-W. Lee, F. Xiong, P.-C. Hsu, Y. Li, J. Zhao, S. Chu, Y. Cui, *Nat. Energy* **2016**, *1*, 16010; b) Q. Xu, Y. Yang, H. Shao, *Phys. Chem. Chem. Phys.* **2015**, *17*, 20398.

[8] a) Y. Liu, D. Lin, Z. Liang, J. Zhao, K. Yan, Y. Cui, *Nat. Commun.* **2016**, *7*, 10992; b) C. Wang, Y. Gong, B. Liu, K. Fu, Y. Yao, E. Hitz, Y. Li, J. Dai, S. Xu, W. Luo, E. D. Wachsman, L. Hu, *Nano Lett.* **2017**, *17*, 565; c) X. Han, Y. Gong, K. Fu, X. He, G. T. Hitz, J. Dai, A. Pearse, B. Liu, H. Wang, G. Rubloff, Y. Mo, V. Thangadurai, E. D. Wachsman, L. Hu, *Nat. Mater.* **2017**, *16*, 572.

[9] a) R. Zhang, X.-R. Chen, X. Chen, X.-B. Chen, X.-Q. Zhang, C. Yan, Q. Zhang, *Angew. Chem. Int. Ed.* **2017**, *56*, 7764; *Angew. Chem.* **2017**, *129*, 7872; b) P. Hao, Z. Zhao, Y. Leng, J. Tian, Y. Sang, R. I. Boughton, C. P. Wong, H. Liu, B. Yang, *Nano Energy* **2015**, *15*, 9; c) Y. Zhang, W. Luo, C. Wang, Y. Li, C. Chen, J. Song, J. Dai, E. M. Hitz, S. Xu, C. Yang, Y. Wang, L. Hu, *Proc. Natl. Acad. Sci. USA* **2017**, *114*, 3584; d) H. K. Kang, S. G. Woo, J. H. Kim, J. S. Yu, S. R. Lee, Y. J. Kim, *ACS Appl. Mater. Interfaces* **2016**, *8*, 26895.

[10] a) Z. Li, M. Shao, L. Zhou, R. Zhang, C. Zhang, J. Han, M. Wei, D. G. Evans, X. Duan, *Nano Energy* **2016**, *20*, 294; b) Z. Li, Q. Yang, K. Fan, W. Xie, W. Qiao, M. Shao, M. Wei, *J. Mater. Chem. A* **2018**, *6*, 21287.

[11] a) B. J. Trześniewski, O. Diaz-Morales, D. A. Vermaas, A. Longo, W. Bras, M. T. M. Koper, W. A. Smith, *J. Am. Chem. Soc.* **2015**, *137*, 15112; b) Z. Li, H. Duan, M. Shao, J. Li, D. O'Hare, M. Wei, Z. L. Wang, *Chem* **2018**, *4*, 2168.

[12] K. Liu, Z. Li, W. Xie, J. Li, D. Rao, M. Shao, B. Zhang, M. Wei, *Energy Storage Mater.* **2018**, *15*, 308.

[13] a) J. Y. C. Chen, L. Dang, H. Liang, W. Bi, J. B. Gerken, S. Jin, E. Ercan Alp, S. S. Stahl, *J. Am. Chem. Soc.* **2015**, *137*, 15090; b) J. Jiang, F. Sun, S. Zhou, W. Hu, H. Zhang, J. Dong, Z. Jiang, J. Zhao, J. Li, W. Yan, M. Wang, *Nat. Commun.* **2018**, *9*, 2885.

Manuscript received: December 29, 2018
Accepted manuscript online: January 25, 2019
Version of record online: February 14, 2019

